INTERNATIONAL JOURNAL FOR NUMERICAL METHODS IN FLUIDS
Int. J. Numer. Meth. Fluids 2008; **56**:305–329
Published online 6 June 2007 in Wiley InterScience (www.interscience.wiley.com). DOI: 10.1002/fld.1527

Prediction of wave pattern and wave resistance of surface piercing bodies by a boundary element method

Sakir Bal*, †

Faculty of Naval Architecture and Ocean Engineering, Istanbul Technical University, Maslak, Istanbul, Turkey

SUMMARY

An iterative boundary element method, which was originally developed for both two- and three-dimensional cavitating hydrofoils moving steadily under a free surface, is modified and extended to predict the wave pattern and wave resistance of surface piercing bodies, such as ship hulls and vertical struts. The iterative nonlinear method, which is based on the Green theorem, allows the separation of the surface piercing body problem and the free-surface problem. The free-surface problem is also separated into two parts; namely, left and right (with respect to x axis) free-surface problems. Those all (three) problems are solved separately, with the effects of one on the other being accounted for in an iterative manner. The wetted surface of the body (ship hull or strut, including cavity surface if exists) and the left and right parts with respect to x axis of free surface are modelled with constant strength dipole and constant strength source panels. In order to prevent upstream waves, the source strengths from some distance in front of the body to the end of the truncated upstream boundary are enforced to be zero. No radiation condition is enforced for downstream and transverse boundaries. A transverse wave cut technique is used for the calculation of wave resistance. The method is first applied to a point source and a three-dimensional submerged cavitating hydrofoil to validate the method and a Wigley hull and a vertical strut to compare the results with those of experiments. Copyright © 2007 John Wiley & Sons, Ltd.

Received 14 November 2006; Revised 16 April 2007; Accepted 17 April 2007

KEY WORDS: wave resistance; ship waves; free surface; vertical strut; boundary element method; potential-based panel method; wave pattern; cavitating vertical hydrofoil; surface piercing strut

INTRODUCTION

Numerical prediction of wave pattern and wave resistance of surface piercing bodies, such as ships, vertical struts and hydrofoils is still of practical importance to engineers and designers. This paper addresses the steady-state characteristics of flow around surface piercing (even unsymmetrical or yawed) bodies. The iterative boundary element (Rankine panel) method (IBEM) developed

*Correspondence to: Sakir Bal, Faculty of Naval Architecture and Ocean Engineering, Istanbul Technical University, Maslak, Istanbul, Turkey.
†E-mail: sbal@itu.edu.tr, URL: http://www.gidb.itu.edu.tr/staff/bal

originally for submerged cavitating hydrofoils moving with a constant speed under a free surface is modified and extended to include the wave pattern and wave characteristics of surface piercing bodies into the calculations.

In the past, theoretical wave resistance was reviewed by Wehausen [1], Newman [2] and more recently by Larsson and Baba [3]. Current trends of ship hydrodynamics including resistance in calm water were also reviewed in [4]. Some historical perspectives and reflections of ship waves are given by Tulin [5], as well. A finite element method for two-dimensional bodies below free surface was described in water of finite depth in [6]. Viscous effects on the free surface has also been considered using the complete Reynolds-averaged Navier–Stokes (RANS) equations in [7, 8]. These, calculations, however, often require the use of a large number of elements (memory) and computation time to achieve adequate resolution of the entire solution domain. Some comparisons of RANS method with experiments and other numerical methods (solutions of potential flow theory) in terms of wave pattern and wave resistance calculations were given in [9, 10]. It was concluded in [10] that the potential flow solution is not yet surpassed for practical applications. However, RANS equations are more promising for future applications.

There are, on the other hand, two groups of boundary integral methods for predicting ship wave resistance: one group is using Kelvin wave source and another one is Rankine source. Emphasis is put on the Rankine panel methods in this paper. One of the very important numerical solution methods that employed a distribution of Rankine type of sources on the ship hull and free surface was introduced by Dawson [11]. This method has increased popularity since then and applied to a wide range of ships. Nakos and Sclavounos [12], however, computed steady wave patterns and wave resistance of several ship hulls, including transom-stern ships by a new Rankine panel method. The fundamental numerical attributes of this method were studied in [13]. Another numerical method based on Rankine sources has been developed for the prediction of flow passing ships in [14]. A desingularized boundary integral method for fully nonlinear free-surface problems was described in [15]. A localized finite element method has been developed to solve the nonlinear free-surface flow around two-dimensional hydrofoils (without cavitation) in [16]. An IBEM (Rankine panel) to solve the flow around surface piercing hydrofoils and ships was presented in [17] as well as two iterative procedures for small and large Froude numbers were presented for fully submerged two-dimensional hydrofoils under a free surface in [18]. The effect of yaw angles for flat plate, on the other hand, was discussed in [19]. Hughes and Bertram in [20] used higher-order Rankine panels as basic elements for ship wave resistance calculations. The former applications (with and without the effect of free surface) of higher-order source panel methods were given for two-dimensional bodies by employing B-splines in [21, 22]. The tunnel wall effects on cavitating hydrofoils without free-surface effect were discussed in [23].

In the present study, however, the IBEM given in [24, 25] is modified and extended to include the surface piercing bodies such as ships and struts into the calculations. This IBEM allows solving the ship hull problem and the free-surface problem separately, with the effects of one problem on the other accounted for by the values of induced potential. This method has several advantages: (1) the solutions of sub-problems are easier to handle and organize than the full problem in terms of numerical implementation; (2) the number of sub-problems (multi hulls problem, appendages, effect of tank walls, etc.) can be increased as much as they are required; and (3) each sub-problem requires less computation time and memory than the solution of full problem. The free-surface problem is also separated into two parts; left (first) and right (second) parts with respect to x axis of free surface, in order to decrease the computation time. Although the number of iterations increases by dividing the free surface into two parts, the overall computation time of the method decreases

DOI: 10.1002/fld

substantially since each iteration step is now very quick. In this way, it is also possible to increase the number of panels on the free surface while keeping the required computation time fixed. The surface piercing body is modelled with constant strength dipole and constant strength source panels, distributed over the body wetted surface. Details of the present low-order potential-based panel method can be found in [26–28]. One of the most important reviews of BEMs up to the late 1970s was given in [29], as well. Both the left and right parts of free surface are also modelled with constant strength dipole and constant strength source panels. The source strengths on both parts of free surface are expressed by using linearized free-surface condition, in terms of the second derivative of perturbation potential with respect to the horizontal axis. Corresponding second-order derivative is calculated by applying the Dawson's fourth-order backward finite difference scheme [11]. Then, two integral equations for unknown perturbation potential values on each part of free surface are obtained by applying Green's theorem. The potential induced by surface piercing body on both parts of free surface, the potential induced by left part of free surface on surface piercing body and right part of free surface, and the potential induced by left part of free surface on surface piercing body and right part of free surface are considered on the right-hand sides of corresponding integral equations. To prevent upstream waves, the first- and second-order derivatives of perturbation potential with respect to horizontal axis are enforced to be equal to zero on the free surface [30]. In order to achieve this, the source strengths on each part of free surface from a distance in front of surface piercing body to the end of truncated upstream boundary are enforced to be equal to zero. No radiation condition is enforced at the transverse and downstream boundaries [31]. In order to calculate the wave resistance of ship, the transverse wave cut method is applied to the downstream waves on the free surface. Details of the method can be found in [32, 33]. The present IBEM is first applied to a constant strength point source and a rectangular cavitating hydrofoil fully submerged under a free surface to validate the method with the one developed before. The IBEM is then applied to a Wigley hull and a rectangular vertical strut and the results are compared with those of experiments given in the literature. The effect of Froude number on the results is discussed.

FORMULATION OF THE PROBLEM

A surface piercing body is subjected to a uniform inflow (U), as shown in Figure 1. The x-axis is positive in the direction of uniform inflow, z-axis is positive upwards and y-axis completes the right-handed system. The undisturbed free surface is located at $z=0$. It is assumed that the fluid is inviscid and incompressible and the flow field is irrotational. Formulation of this problem can be given as in [24, 30] as follows.

Perturbation potential, ϕ and total potential, Φ should satisfy Laplace's equation in the fluid domain:

$$\nabla^2\Phi=\nabla^2\phi=0 \tag{1}$$

Following boundary conditions should also be satisfied by perturbation potential ϕ as follows:

(i) *Kinematic boundary condition on the body surface*: The flow should be tangent to the wetted surface of the body,

$$\frac{\partial\phi}{\partial n}=-\mathbf{U}\cdot\mathbf{n} \tag{2}$$

DOI: 10.1002/fld

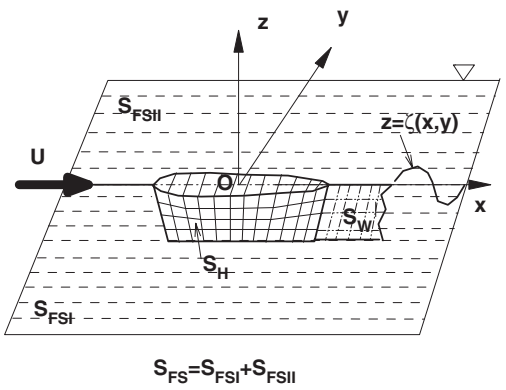

Figure 1. Definition of coordinate system: S_{FSI}, left part of free surface with respect to x axis; S_{FSII}, right part of free surface with respect to x axis.

where **n** is the unit normal vector to the wetted surface of the body, directed into the fluid domain.

(ii) *Kinematic free-surface condition*: The fluid particles should follow the free surface,

$$\frac{DF(x, y, z)}{Dt} = 0 \quad \text{on } z = \zeta(x, y) \tag{3}$$

where $F(x, y, z) = z - \zeta(x, y)$, ζ the free-surface deformation, see Figure 1.

(iii) *Dynamic free-surface condition*: The pressure on the free surface should be equal to the atmospheric pressure (p_{atm}). Applying Bernoulli's equation, the following equation can be obtained:

$$\tfrac{1}{2}[(\nabla\Phi)^2 - U^2] + g\zeta = 0 \quad \text{on } z = \zeta(x, y) \tag{4}$$

where g is the gravitational acceleration.

If Equations (3) and (4) are combined and linearized, then the following free-surface condition can be obtained:

$$\frac{\partial^2\phi}{\partial x^2} + k_0\frac{\partial\phi}{\partial z} = 0 \quad \text{on } z = 0 \tag{5}$$

Here, $k_0 = g/U^2$ is the wave number and corresponding wave elevation can also be given as

$$\zeta = -\frac{U}{g}\frac{\partial\phi}{\partial x} \tag{6}$$

(iv) *Radiation condition*: No upstream waves should occur. In order to prevent upstream waves, both the first and second derivatives of perturbation potential with respect to x is forced to

DOI: 10.1002/fld

be equal to zero for upstream region on the free surface [12, 31]:

$$\frac{\partial^2 \phi}{\partial x^2} = \frac{\partial \phi}{\partial x} = 0 \quad \text{as} \quad x \to -\infty \tag{7}$$

Due to the convective nature of the flow, the upstream boundary condition is the most critical and takes the above form. The origin and the physical interpretations of these two upstream conditions were discussed in more detail in [13] and some numerical experiments on these conditions were given in [34].

(v) *Infinite depth condition*: The perturbation potential should go to zero for infinite depth:

$$\lim_{z \to -\infty} \nabla \phi \to 0 \tag{8}$$

If cavitation occurs on the body, the following boundary conditions should also be satisfied:

(vi) *Dynamic boundary condition on the cavity surface*: The pressure should be constant and equal to p_c (vapour pressure of the fluid) on the cavity surface. Applying Bernoulli's equation, the total velocity, q_c, can be given as [28]

$$q_c = U\sqrt{1+\sigma} \tag{9}$$

where σ is the cavitation number and defined as

$$\sigma = \frac{p - p_c}{(1/2)\rho U^2} \tag{10}$$

(vii) *Kutta condition*: The velocity at the trailing edge of the surface piercing body (or vertical strut) should be finite:

$$\nabla \phi = \text{finite} \quad \text{at the trailing edge} \tag{11}$$

(viii) *Cavity closure condition and cavity height*: The cavity closes at its trailing edge. Refer to [27, 28] for details. On the other hand, cavity detachment point is assumed to be known and in this study the leading edge of the body is chosen as the cavity detachment point:

$$h_c \text{ (cavity height at cavity trailing edge)} = 0 \tag{12}$$

The cavity height (taken normal to the cavity surface) is h_c and determined by integrating the following partial differential equation:

$$\frac{\partial h_c}{\partial s_c}\left[\frac{\partial \Phi}{\partial s_c} - \cos\theta \frac{\partial \Phi}{\partial v_c}\right] + \frac{\partial h_c}{\partial v_c}\left[\frac{\partial \Phi}{\partial v_c} - \cos\theta \frac{\partial \Phi}{\partial s_c}\right] = \sin^2\theta \left[\frac{\partial \phi}{\partial n} + \frac{\partial \Phi_{in}}{\partial n}\right] \tag{13}$$

Here, Φ_{in} is the potential of the uniform incoming flow, s_c and v_c are the curvilinear coordinates on the cavity surface, s_c (chordwise) and v_c (spanwise) direction, and θ is the angle between s_c and v_c. Refer to [28] for details.

On the other hand, to calculate the wave resistance of ship, the transverse wave cut technique originally given by Eggers *et al.* [32] is used here. It is assumed that the wave elevations on the

DOI: 10.1002/fld

free surface with transverse wave cuts can be represented as

$$\zeta(x, y) = \sum_{\upsilon=0}^{\infty} \varepsilon_\upsilon(\alpha_\upsilon \cos\, w_\upsilon x + \beta_\upsilon \sin\, w_\upsilon x)\cos\left(\frac{2\pi\upsilon}{b} y\right) \tag{14}$$

And the associated wave resistance can be given as

$$R_{\mathrm{w}} = \frac{\rho g b}{8} \sum_{\upsilon=0}^{\infty} \varepsilon_\upsilon(\alpha_\upsilon^2 + \beta_\upsilon^2)\left(2 - \frac{k_0}{k_\upsilon}\right) \tag{15}$$

The details of the method and explanations of ε_υ, w_υ, α_υ, β_υ, k_υ and b values can be found in Janson and Spinney [33]. So, it is not repeated here.

NUMERICAL IMPLEMENTATION

According to Green's third identity, the perturbation potential on the ship hull surface and on the free surface can be expressed as

$$2\pi\phi = \int_{S_{\mathrm{FS}}+S_{\mathrm{H}}} \left(\phi \frac{\partial G}{\partial n} - \frac{\partial \phi}{\partial n} G\right) \mathrm{d}S + \int_{S_{\mathrm{W}}} \Delta\phi_{\mathrm{W}} \frac{\partial G}{\partial n^+} \mathrm{d}S \tag{16}$$

where S_{H}, S_{W} and S_{FS} are the boundaries of the surface piercing body, wake and the free surface, respectively. G is the Green function ($G = 1/r$). $\Delta\phi_{\mathrm{W}}$ is the potential jump across the wake surface, and n^+ is the unit vector normal to wake surface pointing upwards. The wake surface leaving the trailing edge of the body along its draft (or its span in case of vertical strut) is located on $y = 0$ plane (see Figure 1). An improved iterative pressure Kutta condition, on the other hand, is applied, where the difference of potentials at the two sides of trailing edge of body is modified, in order to achieve equal pressures at both sides of the trailing edge everywhere along the draft of body (or span in case of vertical strut) [35]. In the present study, the iterative method developed in [24, 25] is applied to solve Equation (16). Iterative method here is composed of three parts: (i) surface piercing body part which solves for the unknown perturbation potential on S_{H}; (ii) left (first) free-surface part which solves for the unknown perturbation potential on S_{FSI}; and (iii) right (second) free-surface part which solves for the unknown perturbation potential on S_{FSII}. Here, $S_{\mathrm{FS}} = S_{\mathrm{FSI}} + S_{\mathrm{FSII}}$ (S_{FSI}: left (first) part of free surface, S_{FSII}: right (second) part of free surface). Here, the free surface is divided into two parts in order to decrease the computation time of the method. Although the number of iterations increases in this way, the overall computation time of the method decreases substantially since each iteration step is now very quick and the method converges generally in two or three iteration steps. In this approach, the method of solution also requires less memory. Potential in the fluid domain due to influence of the surface piercing body, ϕ_{H}, can be given as

$$2\pi\phi_{\mathrm{H}} = \int_{S_{\mathrm{H}}} \left(\phi \frac{\partial G}{\partial n} - \frac{\partial \phi}{\partial n} G\right) \mathrm{d}S + \int_{S_{\mathrm{W}}} \Delta\phi_{\mathrm{W}} \frac{\partial G}{\partial n^+} \mathrm{d}S \tag{17}$$

DOI: 10.1002/fld

Potential in the fluid domain due to the influence of two parts of free surface, ϕ_{FSI} and ϕ_{FSII}, however, can also be given as

$$2\pi\phi_{\mathrm{FSI}} = \int_{S_{\mathrm{FSI}}} \left(\phi \frac{\partial G}{\partial n} - \frac{\partial \phi}{\partial n} G \right) \mathrm{d}S \tag{18}$$

$$2\pi\phi_{\mathrm{FSII}} = \int_{S_{\mathrm{FSII}}} \left(\phi \frac{\partial G}{\partial n} - \frac{\partial \phi}{\partial n} G \right) \mathrm{d}S \tag{19}$$

By substituting Equations (18) and (19) into Equation (16), the following integral equation for the flow on the surface piercing body can be derived:

$$2\pi\phi = \int_{S_{\mathrm{H}}} \left(\phi \frac{\partial G}{\partial n} - \frac{\partial \phi}{\partial n} G \right) \mathrm{d}S + \int_{S_{\mathrm{W}}} \Delta\phi_{\mathrm{W}} \frac{\partial G}{\partial n^{+}} \mathrm{d}S + 4\pi(\phi_{\mathrm{FSI}} + \phi_{\mathrm{FSII}}) \tag{20}$$

and by substituting Equation (19) into Equation (16) similarly, the following integral equations for the flow on the left and right parts of free surface can be derived:

$$2\pi\phi = \int_{S_{\mathrm{FSI}}} \left(\phi \frac{\partial G}{\partial n} - \frac{\partial \phi}{\partial n} G \right) \mathrm{d}S + 4\pi(\phi_{\mathrm{H}} + \phi_{\mathrm{FSII}}) \tag{21}$$

$$2\pi\phi = \int_{S_{\mathrm{FSII}}} \left(\phi \frac{\partial G}{\partial n} - \frac{\partial \phi}{\partial n} G \right) \mathrm{d}S + 4\pi(\phi_{\mathrm{H}} + \phi_{\mathrm{FSI}}) \tag{22}$$

Integral Equations (20)–(22) can be solved iteratively by a low-order panel method with the potentials ϕ_{H}, ϕ_{FSI} and ϕ_{FSII} being updated during the iterative process. Here, the surface piercing body and the parts of free-surface communicate, or 'talk to', each other *via* potential. The flow diagram of this numerical procedure is also shown in Figure 2. After applying kinematic boundary condition, Equations (2)–(20), the following integral equation for the body part can be written:

$$2\pi\phi = \int_{S_{\mathrm{H}}} \left(\phi \frac{\partial G}{\partial n} + (\mathbf{U} \cdot \mathbf{n}) G \right) \mathrm{d}S + \int_{S_{\mathrm{W}}} \Delta\phi_{\mathrm{W}} \frac{\partial G}{\partial n^{+}} \mathrm{d}S + 4\pi(\phi_{\mathrm{FSI}} + \phi_{\mathrm{FSII}}) \tag{23}$$

Similarly, applying the linearized free-surface condition, Equation (5) to Equations (21) and (22), the following integral equations for both parts of free surface can be written:

$$2\pi\phi = \int_{S_{\mathrm{FSI}}} \left(\phi \frac{\partial G}{\partial n} + \frac{1}{k_0} \frac{\partial^2 \phi}{\partial x^2} G \right) \mathrm{d}S + 4\pi(\phi_{\mathrm{H}} + \phi_{\mathrm{FSII}}) \tag{24}$$

$$2\pi\phi = \int_{S_{\mathrm{FSII}}} \left(\phi \frac{\partial G}{\partial n} + \frac{1}{k_0} \frac{\partial^2 \phi}{\partial x^2} G \right) \mathrm{d}S + 4\pi(\phi_{\mathrm{H}} + \phi_{\mathrm{FSI}}) \tag{25}$$

Surface piercing body, Equation (23), and the left and right parts of free surface, Equations (24) and (25), respectively, are discretized into panels with constant strength source and dipole distributions. The discretized integral equations provide three matrix equations, one for surface piercing body and two for free-surface parts, with respect to the unknown potential values. In Equations (24) and (25), the second derivative of perturbation potentials with respect to x is calculated *via* applying the Dawson's original fourth-order backward finite difference scheme [11]. The following can be

DOI: 10.1002/fld

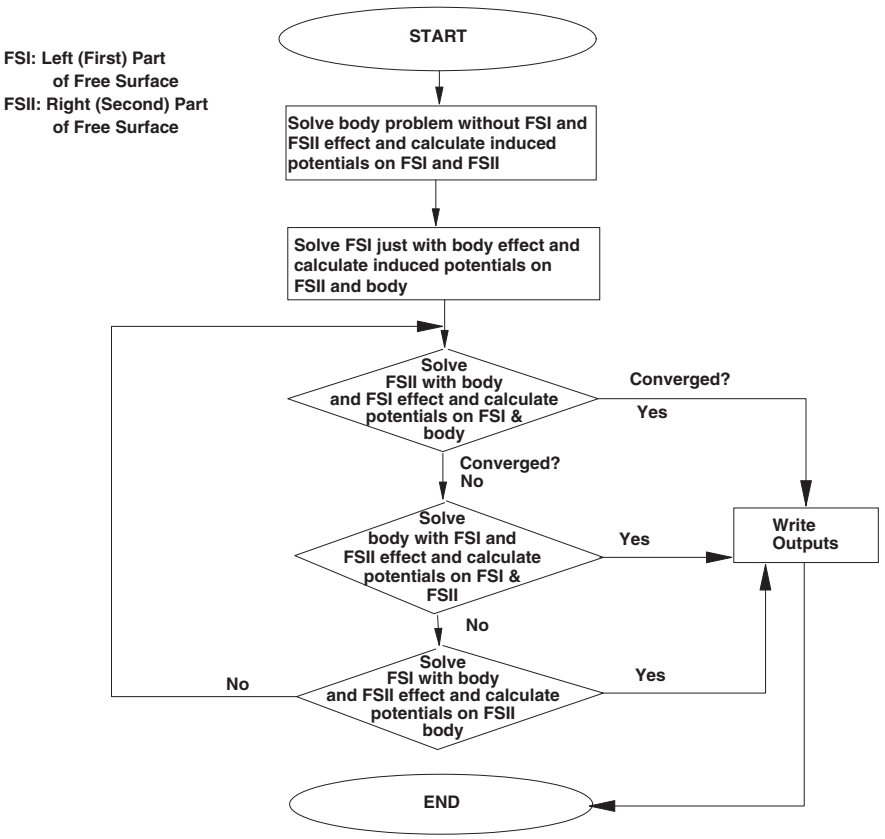

Figure 2. Flow diagram of iterative procedure.

given for any ith panel [24]:

$$\left(\frac{\partial\phi}{\partial x}\right)_i = CA_i\phi_i + CB_i\phi_{i-1} + CC_i\phi_{i-2} + CD_i\phi_{i-3} \tag{26}$$

$$\begin{aligned}\left(\frac{\partial^2\phi}{\partial x^2}\right)_i &= CA_i\phi_i + (CA_iCB_i + CB_iCA_{i-1})\phi_{i-1} \\ &\quad + (CA_iCC_i + CB_iCB_{i-1} + CC_iCA_{i-2})\phi_{i-2} \\ &\quad + (CA_iCD_i + CB_iCC_{i-1} + CC_iCB_{i-2} + CD_iCA_{i-3})\phi_{i-3} \\ &\quad + (CB_iCD_{i-1} + CC_iCC_{i-2} + CD_iCB_{i-3})\phi_{i-4} \\ &\quad + (CC_iCD_{i-2} + CD_iCC_{i-3})\phi_{i-5} + CD_iCD_{i-3}\phi_{i-6}\end{aligned} \tag{27}$$

where the values of CA_i, CB_i, CC_i and CD_i are given in [11] in terms of the spatial discretization.

In order to prevent the upstream waves, the first and second derivatives of perturbation potential ϕ with respect to x are enforced to be equal to zero [12]. It is assumed that the source strengths

DOI: 10.1002/fld

from some distance in front of the ship hull to the upstream truncation boundary on the free surface are equal to zero and which result in $\partial\phi/\partial z$ to be zero. In addition, the smoothing technique that was first introduced by Longuet-Higgins and Cokelet [36] is employed to suppress the development of saw tooth instability on the free surface. The 5-point smoothing formula just for the potential value is applied for each iteration step (between surface piercing body and parts of free surface) to remove the instability as

$$\phi_j^{\text{new}} = \frac{1}{16}(-\phi_{j-2}^{\text{old}} + 4\phi_{j-1}^{\text{old}} + 10\phi_j^{\text{old}} + 4\phi_{j+1}^{\text{old}} - \phi_{j+2}^{\text{old}}) \tag{28}$$

Here, the smoothing formula is only applied in the y direction on the free surface, not in the x direction and ϕ_j^{new} is the new smoothed potential value that is used for calculations.

NUMERICAL RESULTS

First, a point source with constant strength, $1\,\text{m/s}^2$, is chosen to validate the present IBEM. The depth-based Froude number is $(F_h = U/\sqrt{gh} =)$ 1.0 and the submergence depth is $(h = 1.0\,\text{m})$. In Figure 3, wave contours and perspective view of wave deformation on the free surface are shown

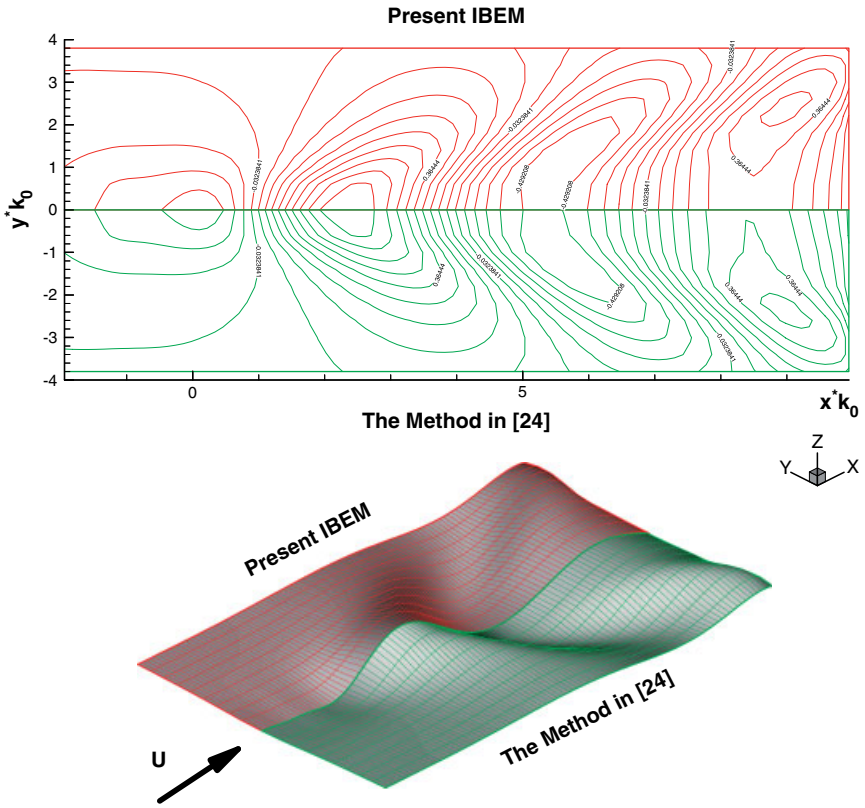

Figure 3. Comparison of wave contours and wave deformation with the method in [24] for point source.

DOI: 10.1002/fld

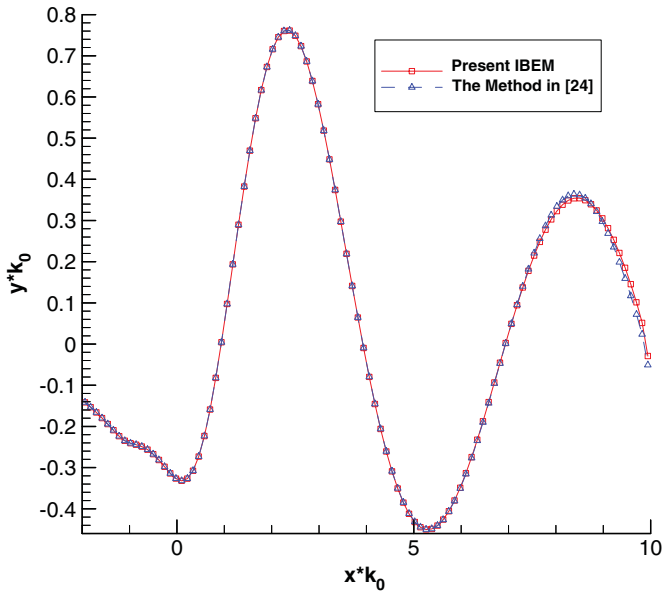

Figure 4. Comparison of wave height with the method in [24] in the middle of free surface for point source.

as compared with those of the method given in [24]. Method given in [24] solves full free-surface problem for submerged point source while present method divides free surface into two parts as explained above. The results of the method given in [24] were also compared with those of the analytical ones and a satisfactory agreement was obtained; see [24, 25]. The number of panels on the free surface is NXFS $*$ (NYFSI + NYFSII) = 100 $*$ (10 + 10) (NXFS is the number of panels along the x direction, NYFSI and NYFSII number of panels in the y direction on the left and right parts of free surface, respectively.) In Figure 4, the wave heights in the middle section (centreline) of the free surface are also shown as compared with those of the method given in [24]. Note that both methods converged to the same values of wave contours and wave heights. In Figure 5, the limits of truncation boundaries (in the transverse and downstream direction) are increased while keeping the total number of panels (NFS = 2000; NFS is the total number of panels on the free surface) fixed on the free surface, so the effect of grid size and truncation of free surface is shown.

Second, a fully submerged cavitating rectangular hydrofoil which has constant NACA0012 profiles along its span (s) is chosen to validate the method. MXPAN3D computer code is used to solve the cavitating hydrofoil problem [28]. The mathematical formulation and solution method for the cavitation part on the hydrofoil surface are given in [28, 30] in detail. Cavitation number, σ, is chosen as 0.4, the angle of attack $\alpha = 5°$, the chord (c) based Froude number $F_c = U/\sqrt{gc} = 1.0$, the ratio of submergence depth of hydrofoil from free surface $h/c = 1.0$. The number of panels used on the hydrofoil surface is NXH $*$ NYH = 40 $*$ 20 (NXH is the number of panels on the hydrofoil surface in the chordwise direction, NYH number of panels in the spanwise direction), the number of panels used on the free surface NXFS $*$ (NYFSI + NYFSII) = 100 $*$ (10 + 10). In Figures 6 and 7, the perspective views of half of cavity shapes by calculated present IBEM are shown as compared with those of method given in [30]. Note that the results of the present IBEM and the

DOI: 10.1002/fld

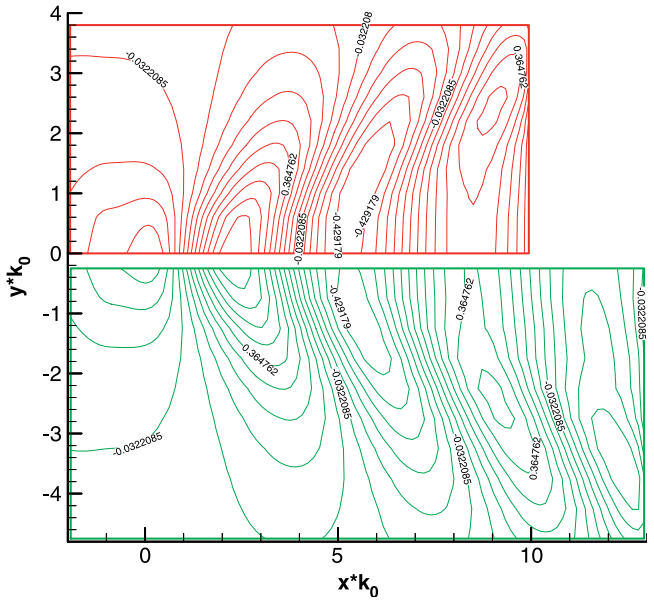

Figure 5. Effect of free-surface truncation and grid size on wave contours for point source, both parts have the same number of panels (NFS = 2000).

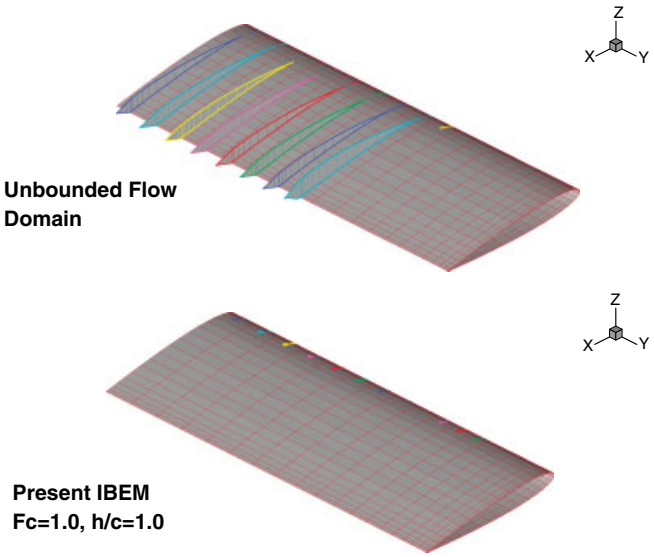

Figure 6. Cavity shapes for half of the hydrofoil as compared with those of unbounded flow domain: $\sigma = 0.4$ and $\alpha = 5^\circ$.

DOI: 10.1002/fld

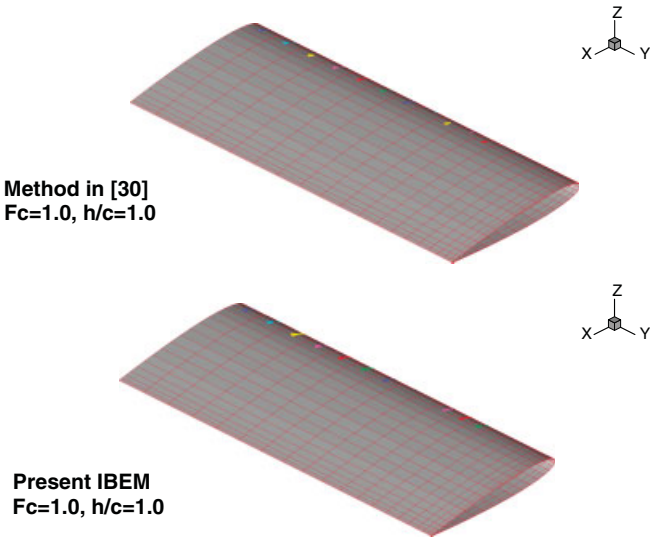

Figure 7. Cavity shapes for half of the hydrofoil as compared with those of method in [30]: $\sigma = 0.4$ and $\alpha = 5°$.

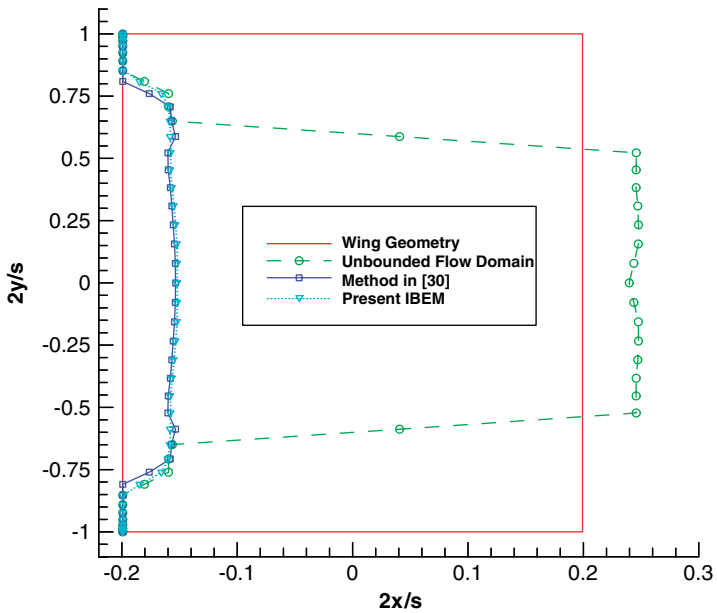

Figure 8. Cavity planforms as compared with those of method in [30]: $\sigma = 0.4$, $\alpha = 5°$, $F_c = 1.0$, $h/c = 1.0$.

method given in [30] are converged to the same values. This can be seen much clearly in Figure 8 that the cavity planforms are shown. The method given in [30] solves full free surface problem in a similar way for the point source while present IBEM separates the free surface into two parts as

DOI: 10.1002/fld

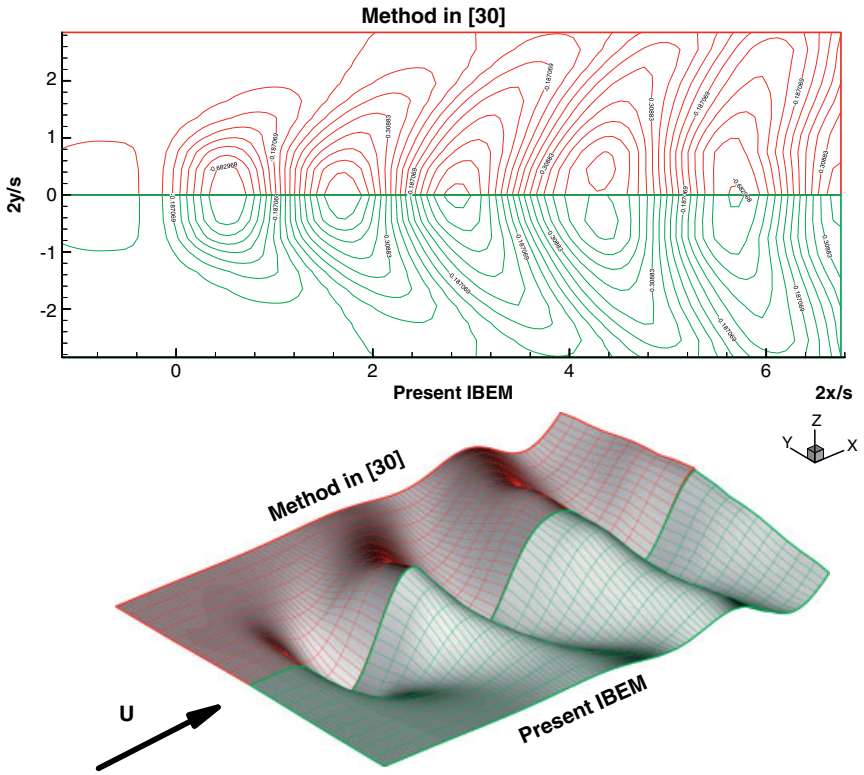

Figure 9. Comparison of wave contours and wave deformation with those of method in [30]: $\sigma = 0.4$, $\alpha = 5^\circ$, $F_c = 1.0$, $h/c = 1.0$.

explained above. The cavity planform and shapes are also added to Figures 6 and 8 in unbounded flow domain (no free surface effect). Note also that the free surface caused shorter cavity lengths (and cavity volume) for this particular case. In Figure 9, a comparison of wave contours and wave deformation on the free surface with those of the method given in [30] is shown. Both methods converged to the same values of wave contours.

Third, the IBEM is applied to a Wigley hull to compare the results with those of experiments given in [12, 13]. Chosen hull has a length-to-beam ratio of 10 and a beam-to-draft ratio of 1.6 and the following equation for the hull surface:

$$y = \pm \frac{B}{2}\left[1 - \left(\frac{2x}{L}\right)^2\right]\left[1 - \left(\frac{z}{H}\right)^2\right] \tag{29}$$

where L is the length, B the beam and H the draft. The perspective view of the panels used both on the hull surface and free surface is illustrated in Figures 10 and 11. NXFS = 100, NYFS = NYFSI+ NYFSII = 10 + 10 = 20 (total number of panels on the free surface is NFS = 100 * 20 = 2000), NXH = 90, NYH = 20 (total number of panels on the hull surface NHULL = 2 * 90 * 20 = 3600) are used for all calculations performed for Wigley hull. Half of the wave contours and wave

DOI: 10.1002/fld

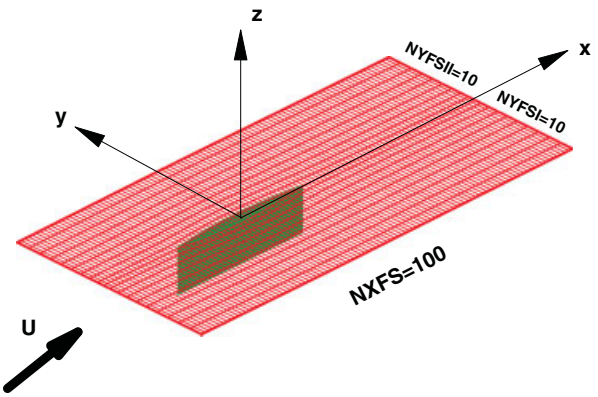

Figure 10. Perspective view of panels used on the free surface and Wigley hull surface.

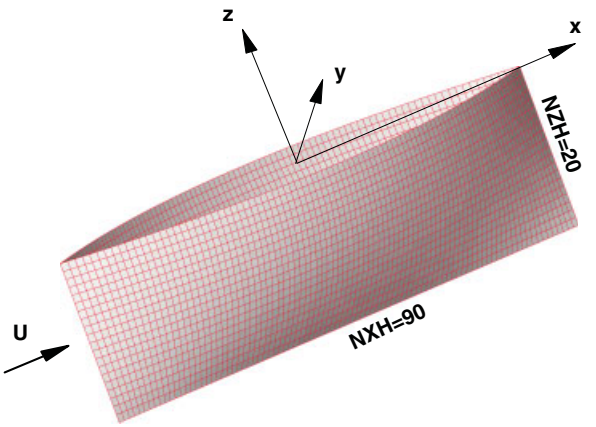

Figure 11. Perspective view of panels used on the Wigley hull surface.

deformations on the free surface for Froude numbers ($Fn = U/\sqrt{gL}$) = 0.2, 0.3 and 0.4 are shown in Figures 12(a), 13(a) and 14(a), respectively. The wave contours for $Fn = 0.2$, 0.3 and 0.4 taken from [12] are also illustrated to compare the results of present IBEM with those of [12] in Figures 12(b), 13(b) and 14(b), respectively. Note that the wave contours are consistent with those of Nakos and Sclavounos [12] and show a compatible variation with respect to the Froude number. In Figure 15, the predicted values of wave resistance by the technique of transverse wave cuts on the free surface are compared with those of experiments (model fixed case) given by Nakos and Sclavounos [12]. The wave resistance curve shows compatible variation with respect to the Froude number and is consistent with the experimental measurements.

The present IBEM is then applied to a rectangular vertical strut (hydrofoil) which has constant NACA63A009 sections along its spanwise direction. Span/chord ratio and the angle of attack are

DOI: 10.1002/fld

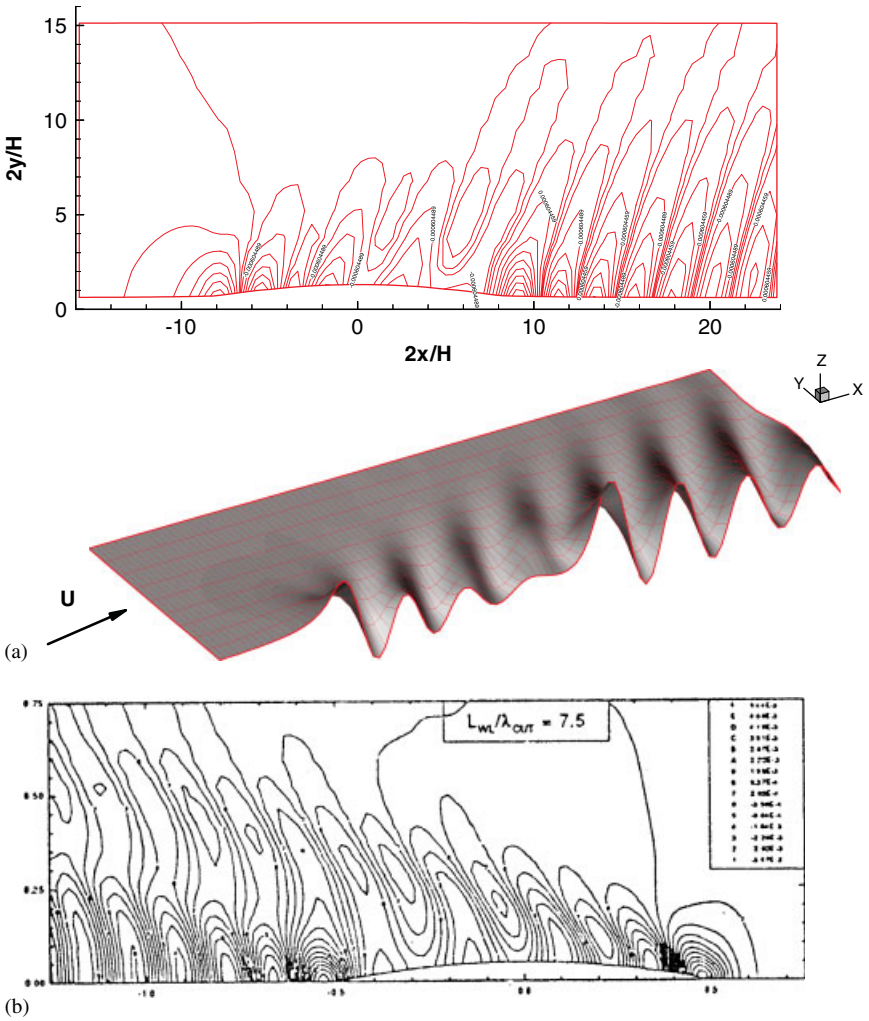

Figure 12. (a) Wave contours and deformation on the free surface for Wigley hull, $Fn = 0.2$ and (b) wave contours for Wigley hull, $Fn = 0.2$, taken from [12].

chosen as $s/c = 1.8$ and $\alpha = 4^\circ$ to compare the results with those of experiments given in [17]. In Figures 16 and 17, the perspective views of the panels used both on the vertical strut (hydrofoil) surface and free surface are illustrated. NXFS = 100, NYFS = NYFSI + NYFSII = 10 + 10 = 20 (total number of panels on the free surface is NFS = 100 * 20 = 2000), NXH = 80, NYH = 20 (total number of panels on the strut surface NHULL = 80 * 20 = 1600) are used for all calculations of vertical strut. The calculated non-dimensional lift coefficient values by the present method *versus* angle of attack are compared with those of experimental measurements and another numerical method for Froude numbers $F_c = U/\sqrt{gc} = (0.5$ and $1.0)$, in Figures 18 and 19, respectively [17]. The lift coefficient values are calculated by the integration of pressure over the strut surface.

DOI: 10.1002/fld

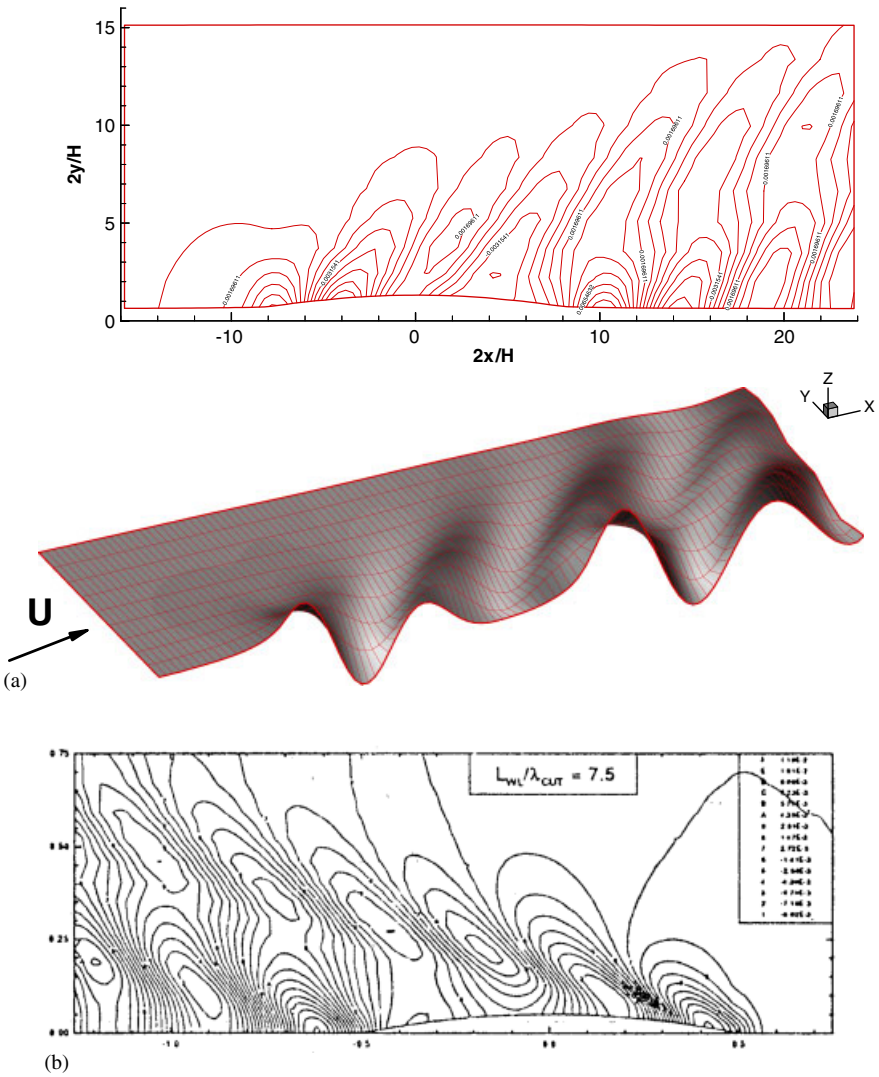

Figure 13. (a) Wave contours and deformation on the free surface for Wigley hull, $Fn = 0.3$ and (b) wave contours for Wigley hull, $Fn = 0.3$, taken from [12].

Although the experimental lift value is higher than the calculated one by the present method for $F_c = 0.5$ and $\alpha = 4°$, the agreement between the results of experimental measurements and the present numerical method is satisfactory. The drag coefficient values (wave drag + induced drag) by the present method are also shown for both Froude numbers ($F_c = 0.5$ and 1.0) in Figure 20. In Figures 21 and 22, the wave contours and wave deformation on the free surface are given for chord-based Froude numbers (F_c defined above) 0.5 and 1.0, respectively. In Figures 23 and 24, the non-dimensional pressure distributions (contours) on the back and face sides of vertical strut are shown for $F_c = 1.0$, respectively. In Figure 25, the convergence history of the present IBEM

DOI: 10.1002/fld

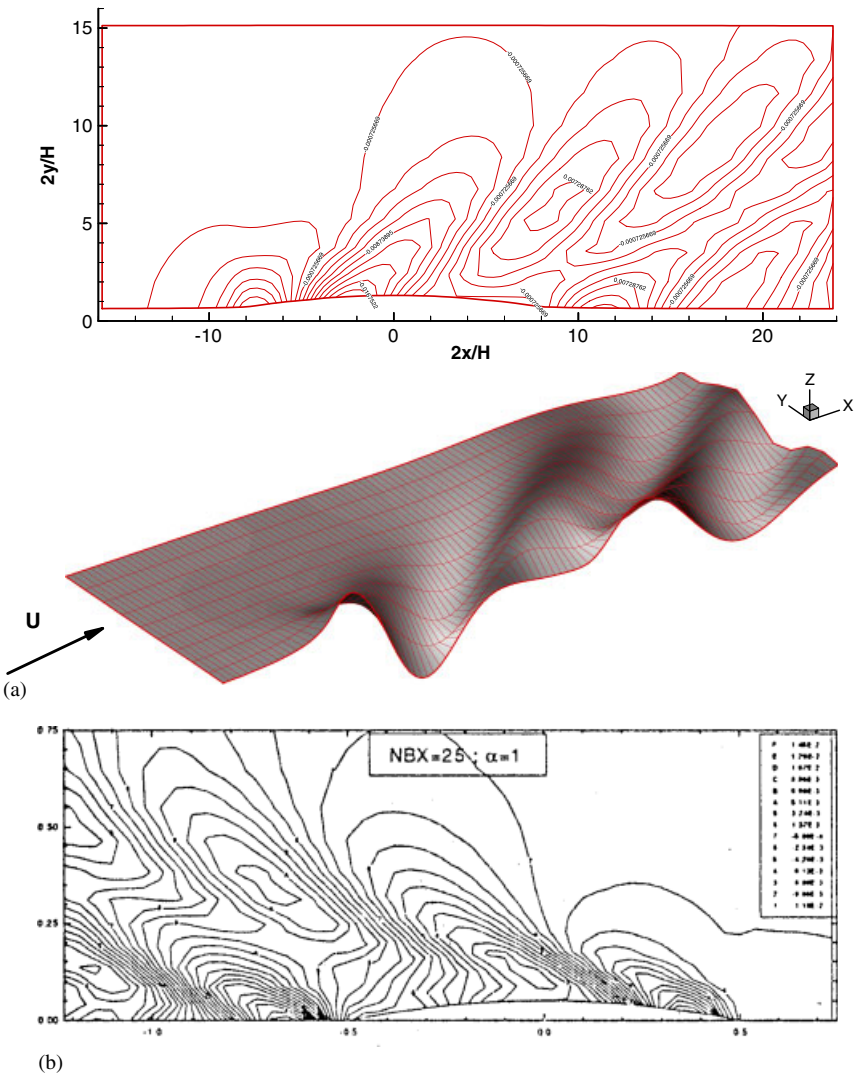

Figure 14. (a) Wave contours and deformation on the free surface for Wigley hull, $Fn = 0.4$ and (b) wave contours for Wigley hull, $Fn = 0.4$, taken from [12].

on the wave heights in the middle of free surface is shown with iteration steps. Note the quick convergence of the method; the second iteration is the converged solution.

CONCLUSIONS AND FUTURE WORK

An IBEM for surface piercing bodies moving with a constant speed on the free surface was described. The iterative method was based on the perturbation potential formulation. The surface

DOI: 10.1002/fld

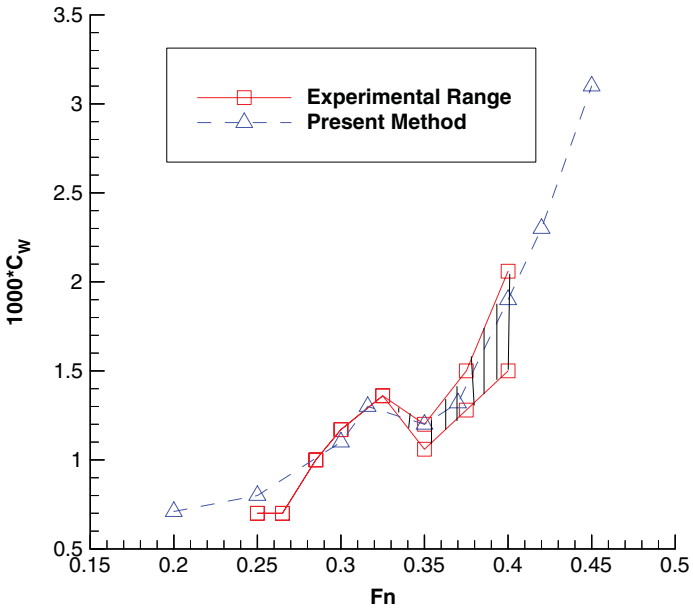

Figure 15. Comparison of predicted wave resistance values with those of experiments taken from [12] for Wigley hull.

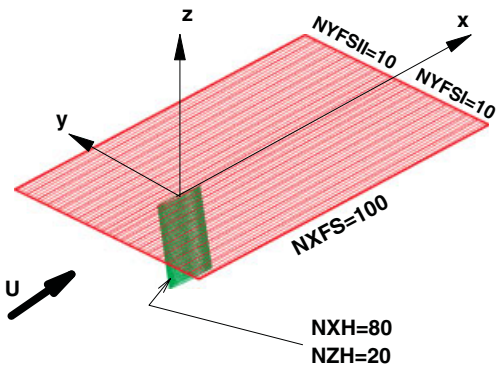

Figure 16. Perspective view of panels used on the free surface and vertical hydrofoil surface.

piercing body and the free-surface part of the problem were solved, separately, with the effects of one on the other taken into account iteratively. The free-surface problem was also separated into two parts to decrease the computation time and the memory requirement. These (three) problems communicate, or 'talk to', each other *via* potential. The method was first applied to a constant strength point source and a fully submerged cavitating hydrofoil to validate the method with the previous method given in [24]. It is found that the method given in detail in [24] and the present IBEM converged to the same results. The present IBEM later applied to a Wigley hull and a vertical strut (hydrofoil) to compare the results with those of experiments. It is found that the wave

DOI: 10.1002/fld

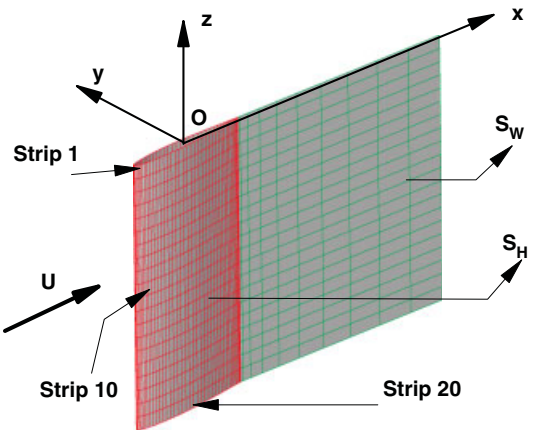

Figure 17. Perspective view of panels used on the vertical hydrofoil surface.

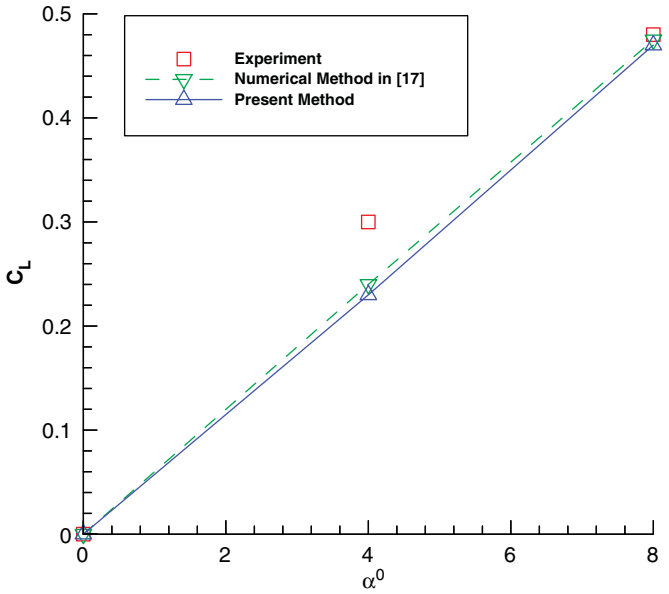

Figure 18. Non-dimensional lift coefficient values *versus* angle of attack for $F_c = 0.5$.

pattern by the present method are compatible with Froude numbers and the transverse wave cut technique using the predicted wave deformations by the present method calculates satisfactorily the wave resistance values over the entire Froude range and the wave resistance curve is consistent with that of the experimental measurements. It is also found that the present method can predict the wave pattern and the lift and drag coefficient values (wave drag + induced drag + cavity drag if exists) of vertical struts with yaw angles with and without cavitation. Present IBEM also converges very quickly (within two or three iteration steps). This IBEM can be modified to deal with

DOI: 10.1002/fld

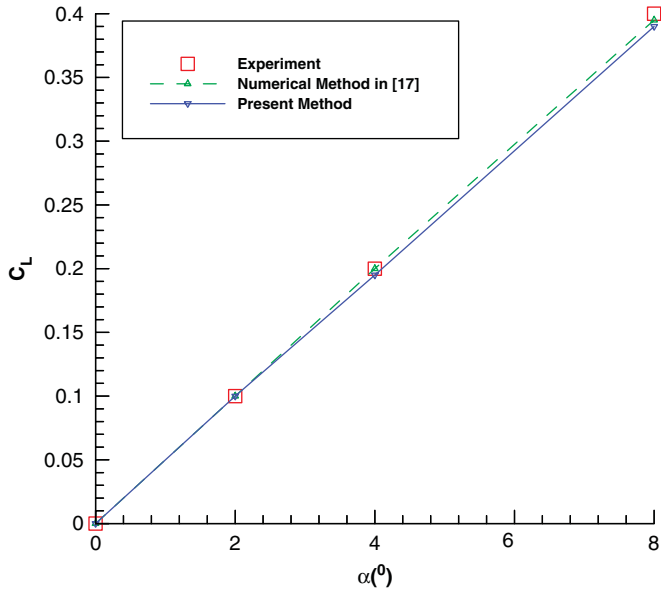

Figure 19. Non-dimensional lift coefficient values *versus* angle of attack for $F_c = 1.0$.

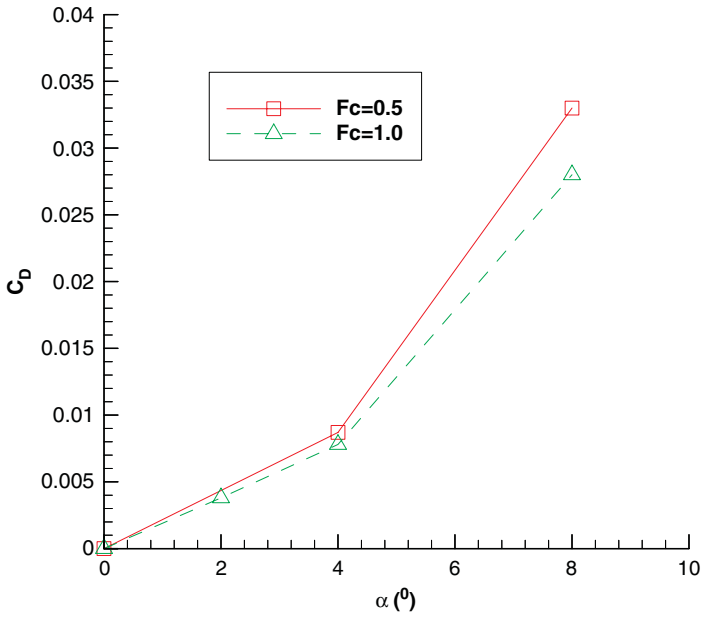

Figure 20. Non-dimensional drag coefficient values *versus* angle of attack for $F_c = 1.0$ and 0.5.

DOI: 10.1002/fld

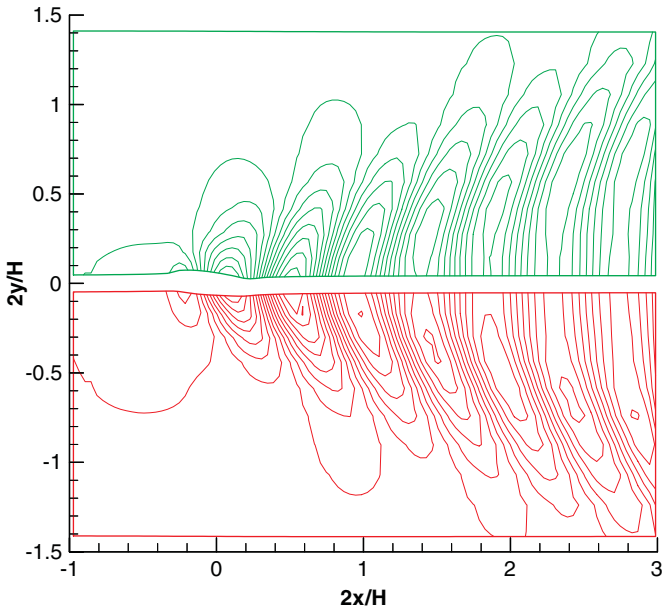

Figure 21. Wave contours for vertical hydrofoil with 4° yaw angle, for $Fn = 0.5$.

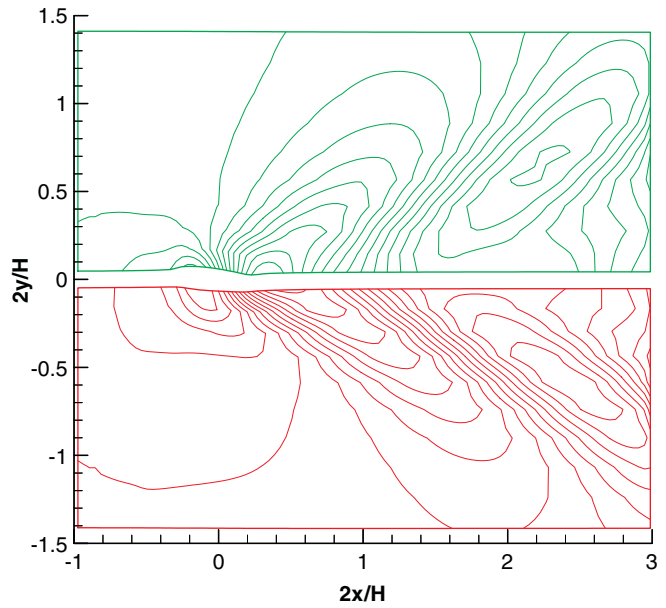

Figure 22. Wave contours for vertical hydrofoil with 4° yaw angle, for $Fn = 1.0$.

DOI: 10.1002/fld

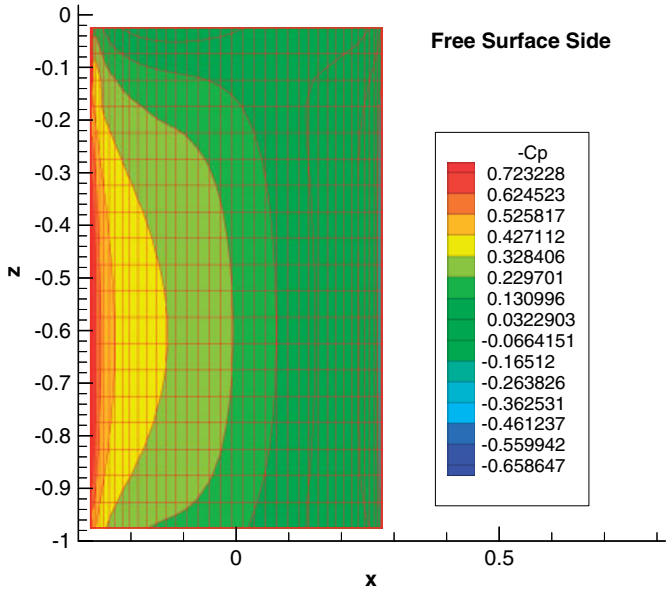

Figure 23. Pressure distribution on back side of hydrofoil, for $F_c = 1.0$.

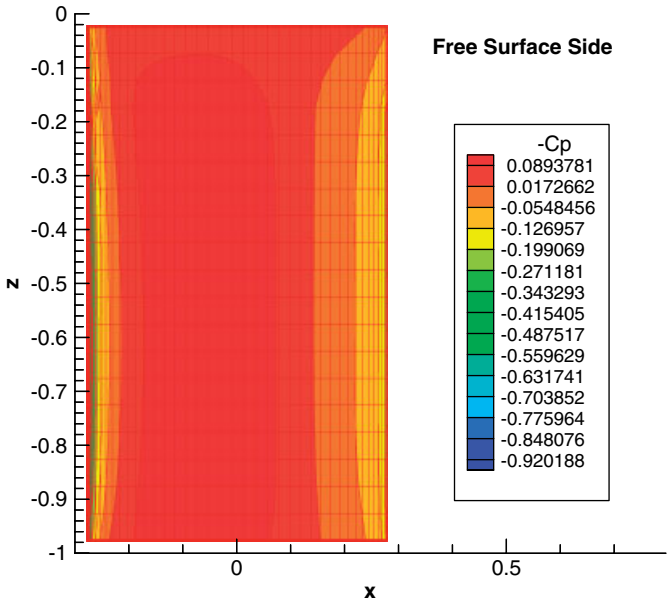

Figure 24. Pressure distribution on face side of hydrofoil, for $F_c = 1.0$.

DOI: 10.1002/fld

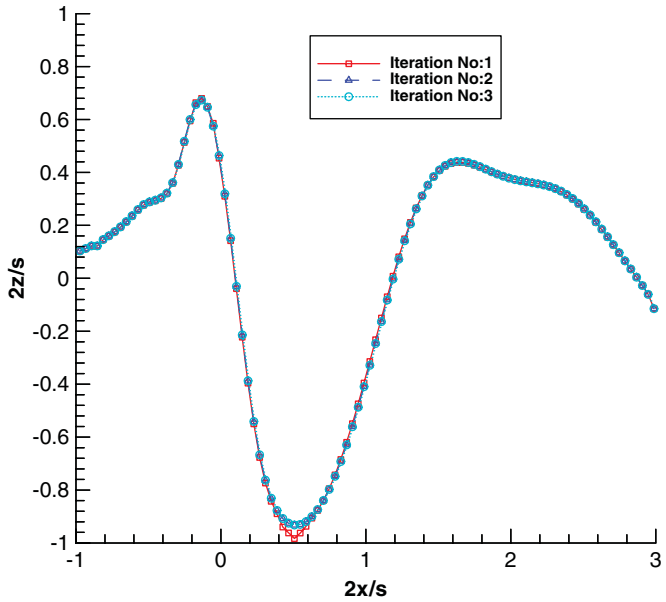

Figure 25. Convergence history of wave heights in the middle of free surface, with iteration steps.

multi-surface piercing ship hulls and/or struts; such as catamarans or trimarans. The effects of walls of a numerical towing tank can also be included into the present calculations in a similar way given by Bal and Kinnas [37]. For transom sterns, this method can be improved by adding wake strips of panels in the downstream direction and by enforcing smooth detachment conditions as presented in [12]. An explicit nonlinear pressure Kutta condition can also be applied for hulls with deeper transoms and/or fuller aft bodies which result in significant cross-flow velocities. Such an approach was successfully implemented for steady and unsteady flows in [35, 38].

ACKNOWLEDGEMENTS

The author would like to thank the referees for their constructive comments.

REFERENCES

1. Wehausen JV. The wave resistance of ships. *Advances in Applied Mechanics* 1973; **13**:93–245.
2. Newman JN. *Marine Hydrodynamics*. MIT Press: Cambridge, MA, U.S.A., 1977.
3. Larrson L, Baba E. *Ship Resistance and Flow Computations*. Advances in Marine Hydrodynamics. Computational Mechanics Publications: Southampton, 1996; 1–76.
4. Bulgarelli UP, Lugni C, Landrini M. Numerical modeling of free surface flows in ship hydrodynamics. *International Journal for Numerical Methods in Fluids* 2003; **43**:465–481.
5. Tulin MP. Reminiscences and reflections: ship waves, 1950–2000. *Journal of Ship Research* 2005; **49**(4):238–246.
6. Kim JW, Bai KJ. A finite element method for two-dimensional water-wave problems. *International Journal for Numerical Methods in Fluids* 1999; **30**:105–121.
7. Miyata H, Zhu M, Watanabe O. Numerical study on a viscous flow with free surface waves about a ship in steady straight course by a finite volume method. *Journal of Ship Research* 1992; **36**(4):332–345.

DOI: 10.1002/fld

8. Farmer J, Martinelli L, Jameson A. Fast multigrid method for solving incompressible hydrodynamic problems with free surfaces. *AIAA Journal* 1994; **32**(6):1175–1182.
9. Chen HC, Lee SK. RANS/Laplace calculations of nonlinear waves induced by surface-piercing bodies. *Journal of Engineering Mechanics* 1999; **125**(11):1231–1242.
10. Gatchell S, Hafermann D, Jensen G, Marzi J, Vogt M. Wave resistance computations—a comparison of different approaches. *Proceedings of the 23rd Symposium on Naval Hydrodynamics*, Val de Reuil, France, 2001.
11. Dawson DW. A practical computer method for solving ship-wave problems. *Proceedings of the 2nd International Conference on Numerical Ship Hydrodynamics*, U.S.A., 1977.
12. Nakos DE, Sclavounos PD. Kelvin wakes and wave resistance of cruiser- and transom-stern ships. *Journal of Ship Research* 1994; **38**:9–29.
13. Sclavounos PD, Nakos DE. Stability analysis of panel methods for free surface flows with forward speed. *Proceedings of the 17th Symposium on Naval Hydrodynamics*, Netherlands, 1988.
14. Rigby SG, Nicolaou D, Sproston JL, Millward A. Numerical modeling of the water flow around ship hulls. *Journal of Ship Research* 2001; **45**(2):85–94.
15. Cao Y, Schultz WW, Beck RF. Three-dimensional desingularized boundary integral methods for potential problems. *International Journal for Numerical Methods in Fluids* 1991; **12**:785–803.
16. Bai JK, Han JH. A localized finite element method for the nonlinear steady waves due to a two-dimensional hydrofoil. *Journal of Ship Research* 1994; **38**:42–51.
17. Hsin CY, Chou SK. Applications of a hybrid boundary element method to the analysis of free surface flow around lifting and nonlifting bodies. *Proceedings of the 22nd Symposium on Naval Hydrodynamics*, Washington, DC, U.S.A., 1998.
18. Yasko M. Boundary element method for a hydrofoil near the free surface. *Engineering Analysis with Boundary Elements* 1998; **21**:191–194.
19. Maniar H, Newman JN, Xu H. Free surface effects on a yawed surface piercing plate. *Proceedings of the 18th Symposium on Naval Hydrodynamics*, Ann Arbor, MI, U.S.A., 1990.
20. Hughes M, Bertram V. A higher-order panel method for 3-D free surface flows. *Report No. 558*, Institut für Schiffbau der Universitat Hamburg, October 1995.
21. Okan MB, Umpleby SM. The use of B-splines for the calculation of two-dimensional potential flow around arbitrary bodies. *International Shipbuilding Progress* 1985; **32**:151–155.
22. Okan MB, Umpleby SM. Free surface flow around arbitrary two-dimensional bodies by B-splines. *International Shipbuilding Progress* 1985; **32**:182–187.
23. Choi JK, Kinnas SA. Numerical water tunnel in two- and three-dimensions. *Journal of Ship Research* 1998; **42**:86–98.
24. Bal S, Kinnas SA, Lee H. Numerical analysis of 2-D and 3-D cavitating hydrofoils under a free surface. *Journal of Ship Research* 2001; **45**(1):34–49.
25. Bal S, Kinnas SA. A BEM for cavitating hydrofoils under a free surface. *Proceedings of the IABEM-2000 Symposium*, Brescia, Italy, 2000; 13–17.
26. Brebbia CA, Telles JCF, Wrobel LC. *Boundary Element Techniques—Theory and Applications in Engineering*. Springer: Berlin, 1984.
27. Kinnas SA, Fine NE. Nonlinear analysis of the flow around partially or supercavitating hydrofoils by a potential based panel method. *Proceedings of the IABEM-90 Symposium*, Rome, Italy, 1991; 289–300.
28. Kinnas SA, Fine NE. A numerical nonlinear analysis of the flow around two- and three-dimensional partially cavitating hydrofoils. *Journal of Fluid Mechanics* 1993; **254**:151–181.
29. Cheng AHD, Cheng DT. Heritage, early history of the boundary element method. *Engineering Analysis with Boundary Elements* 2005; **29**:268–302.
30. Bal S. Kinnas SA. A BEM for the prediction of free surface effects on cavitating hydrofoils. *Computational Mechanics* 2002; **28**:260–274.
31. Nakos DE, Sclavounos PD. On steady and unsteady ship wave patterns. *Journal of Fluid Mechanics* 1990; **215**:263–288.
32. Eggers KWH, Sharma SD, Ward LW. An assessment of some experimental methods for determining the wavemaking characteristics of a ship form. *Transactions of SNAME* 1967; **75**:112–157.
33. Janson CE, Spinney D. A comparison of four wave cut analysis methods for wave resistance prediction. *Ship Technology and Research* 2004; **51**:173–184.
34. Bal S. Numerical analysis of cavitating hydrofoils under a free surface. *Report No. 99-5*, Ocean Engineering Group, Department of Civil Engineering, The University of Texas at Austin, U.S.A., 1999.

DOI: 10.1002/fld

35. Kinnas SA, Hsin C. A boundary element method for the analysis of the unsteady flow around extreme propeller geometries. *AIAA Journal* 1992; **30**(3):688–696.
36. Longuet-Higgins MS, Cokelet ED. The deformation of steep surface waves on water (I)—a numerical method of computation. *Proceedings of Royal Society of London*, *Series A* 1976; **350**:1–26.
37. Bal S, Kinnas SA. A numerical wave tank model for cavitating hydrofoils. *Computational Mechanics* 2003; **32**:259–268.
38. Kinnas SA, Hsin CY, Keenan D. A potential based panel method for the unsteady flow around open and ducted propellers. *Proceedings of the 18th Symposium on Naval Hydrodynamics*, Ann Arbor, MI, U.S.A., 1990.

DOI: 10.1002/fld